

# Invasion with stage-structured coupled map lattices: Application to the spread of scentless chamomile

T. de-Camino-Beck<sup>a,\*</sup>, M.A. Lewis<sup>a,b</sup>

<sup>a</sup> Centre for Mathematical Biology, Department of Mathematical and Statistical Sciences, University of Alberta, Edmonton, Alberta T6G 2G1, Canada

<sup>b</sup> Department of Biological Sciences, University of Alberta, Edmonton, Alberta T6G 2E9, Canada

## ARTICLE INFO

### Article history:

Received 17 August 2008

Received in revised form 31 August 2009

Accepted 4 September 2009

Available online 14 October 2009

### Keywords:

Coupled map lattice

Wave speed

Rate of spread

Biological control

## ABSTRACT

Two fundamental aspects of invasion dynamics are population growth and population spread. These quantities have been subject of study in biological invasions and can be used to study management and control of organisms. In this paper we derive formulae to calculate wave speed and rates of spread for coupled map lattices. Coupled map lattice models are dynamical models where space and time are discrete. We also show how wave speed and rate of spread can be calculated for structured population coupled map lattices in deterministic, stochastic environments and heterogeneous landscapes. Coupled map lattices are simple mathematical models that can be easily linked to landscape data to study invading organisms control strategies.

© 2009 Elsevier B.V. All rights reserved.

## 1. Introduction

Two fundamental aspects of invasion dynamics are population growth and population spread. The two related quantities (intrinsic growth rate and rate of spread) are essential to invasion theory. They have been the subject of study in mathematical models for invasions (Hastings et al., 2005), and the quantities are key control parameters in conservation management and biological control (Fagan et al., 2002; Shea, 2004; Neubert and Parker, 2004; Allen et al., 1996). Because of the long time and broad spatial scales at which invasions occur, the use of models is essential to understand the dynamics of invasions and design possible management and conservation strategies.

There are several modelling strategies for population growth and spatial spread: partial differential equations, integro-difference equations, coupled map lattices, and cellular automata. Partial differential equations incorporate continuous space and time, integro-difference equations, discrete time and continuous space, and coupled map lattice, discrete time and space. For cellular automata, in addition to time and space being discrete, the state space is also discrete. Which modelling strategy is the best depends upon the dynamical characteristics of the system under analysis, and upon spatio-temporal scales. In the last

two decades there has been an increase in the use of discrete models due to their ability to incorporate stochastic components and local inhomogeneities (Durrett and Levin, 1994), and because personal computers now allow for fast numerical computations.

Integro-difference equation (IDE) models are discrete-time and continuous-space models, that incorporate dispersal data directly using a kernel function (Kot et al., 1996). This dispersal kernel allows for the redistribution of individuals in continuous space. These models have been widely used to study spatial dynamics and control of invasive species (e.g. Allen et al., 1996; Buckley et al., 2005; Kot et al., 1996). Mathematically an IDE is defined as

$$n_{t+1}(x) = \int_{-\infty}^{\infty} \underbrace{k(x, y)}_{\text{dispersal from } y \text{ to } x} \underbrace{f[n_t(y)]}_{\text{growth at } y} dy. \quad (1)$$

Here  $n_t(x)$  is population density at time  $t$  location  $x$  and  $f[n_t(y)]$  describes population growth. The dispersal kernel  $k(x, y)$  is a probability density function describing the likelihood of dispersal to point  $x$ .

Coupled map lattices (CMLs) are models where space and time are discrete, and whose structure is similar to IDEs. Some CMLs have been used to study host–parasitoid interactions (Hassell et al., 1991; Kean and Barlow, 2001; Bjornstad and Bascombe, 2001; Bonsall and Hassell, 2000), metapopulation level applications (Janosi and Scheuring, 1997), applied biological control (Rees and Paynter, 1997; Rees and Hill, 2001), and tree dispersal (Jiang and Zhang, 2008). A coupled map lattice is a dynamical system where

\* Corresponding author. Current address: Depts. of Entomology and Biology, Penn State University, State College, PA 16802, USA. Fax: +1 780 492 6826.

E-mail addresses: [tomasd@psu.edu](mailto:tomasd@psu.edu) (T. de-Camino-Beck), [mlewis@math.ualberta.ca](mailto:mlewis@math.ualberta.ca) (M.A. Lewis).

time and space are discrete, and the state variable is continuous (White and White, 2005; Kaneko, 1992).

As with integro-difference equations, a CML describes the growth and dispersal of the population, but now on a discrete lattice. Strictly, a CML only involves local interactions, meaning dispersal occurs in a local neighbourhood  $\Omega$ . However, there is no restriction on how large  $\Omega$  is. Consider the continuous spatial domain  $\bar{X}$ . A one-dimensional discrete regular lattice over  $\bar{X}$  is defined as  $X = \{x_{-\infty}, \dots, x_0, \dots, x_{\infty}\}$ , with  $x_i = ih$ , where  $h$  is the cell size (scale) of the lattice and  $i$  is an integer. Mathematically a CML can be defined,

$$n_{t+1}(x_i) = \sum_{x_j \in \Omega} \underbrace{k(x_i, x_j)}_{\text{dispersal from } x_j \text{ to } x_i} \underbrace{f[n_t(x_j)]}_{\text{growth at } x_j} \quad (2)$$

where  $x_i, x_j$  are points in a one-dimensional lattice,  $n_t(x_i)$  is population at time  $t$  location  $x_i$ ,  $f[n_t(x_i)]$  is a map that models population growth and  $k(x_i, x_j)$  is a discrete probability mass function for dispersal. In a spatially homogeneous environment, dispersal kernels that only depend on signed distance  $x_d = x_i - x_j$  are called difference kernels. As an example of a difference kernel  $k(x_d)$ ,  $x_d = x_i - x_j$ , consider,

$$k(x_d) = \begin{cases} (1 - u) & \text{if } x_d = 0 \\ \frac{u}{|\Omega| - 1} & \text{otherwise} \end{cases} \quad (3)$$

where  $|\Omega|$  is the number of cells in the neighbourhood  $\Omega$ . Note that  $u \in [0, 1]$  and  $\sum_{\Omega} k(x_d) = 1$ . When  $|\Omega| = 3$ , this example is considered a classic CML model with nearest neighbour interaction. CMLs can be extended to a two-dimensional spatial lattice. Here the nearest neighbour interactions, in a Moore neighbourhood, involve the central lattice point and eight neighbours so that  $|\Omega| = 9$ .

Some comparative studies show how results can be obtained using CMLs are similar to those found with other modelling structures like IDEs and individual-based models (White and White, 2005; Brannstrom and Sumpter, 2005). As we will show here, analytical tools developed for IDEs can be used directly to study spread in discrete space for structured population models.

In this paper we apply tools developed for calculation of wave speed and spread rate in integro-difference equations to coupled map lattices. To our knowledge, the application of these to CMLs is new. We use CMLs to study the population dynamics and spread of structured populations with applications to a particular invader, scentless chamomile (*Matricaria perforata*), an introduced annual, biennial or short-lived perennial plant that has become a widely distributed weed in cultivated areas in North America (Hinz, 1996; Hinz and McClay, 2000). We further analyze possible control strategies, and explore CMLs in heterogeneous landscapes and stochastic environments.

## 2. Discrete structured spatial models

### 2.1. Matrix coupled map lattice equations

Matrix population models have been shown to be an effective tool to study population growth and control (Shea and Kelly, 1998; van den Driessche and Watmough, 2002; Parker, 2000; McLeod and Saunders, 2001). Space can be incorporated in the matrix model formulation by extending a structured population across space, and considering dispersal between these locations in a continuous or discrete domain. Here we consider stage-structured models with discrete space which we will call Matrix CML. For continuous space stage-structured models see Neubert and Caswell (2000). A matrix

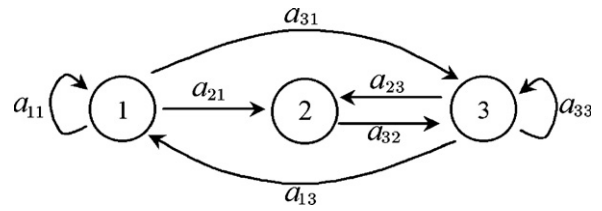


Fig. 1. Life cycle graph of scentless chamomile. Node 1: seed bank, node 2: rosettes, and node 3: flowering plants.

CML equation with stage structure is described by

$$\mathbf{n}_{t+1}(x_i) = \sum_{x_j \in \Omega} [\tilde{\mathbf{K}}(x_i, x_j) \circ \mathbf{A}] \mathbf{n}_t(x_j) \quad (4)$$

Here  $\mathbf{A}$  is the projection matrix,  $\mathbf{n}_t(x_i)$  is a vector of stages at time  $t$  location  $x_i$  and  $\tilde{\mathbf{K}}$  is a matrix of discrete kernels whose elements  $\tilde{k}_{lm}(x, y)$  are kernels that describe dispersal as the individual moves from location  $y$  to  $x$  from stage  $m$  to stage  $l$ . Each entry of  $\tilde{\mathbf{K}}(x_i, x_j) = [\tilde{k}_{lm}(x_i, x_j)]$  must satisfy:

$$\sum_{i=-\infty}^{\infty} \tilde{k}_{lm}(x_i, x_j) = 1, \quad (5)$$

If difference kernels are assumed then  $\tilde{\mathbf{K}}(x_i - x_j)$ . The symbol “ $\circ$ ” denotes Hadamard product which is element-wise multiplication. It is assumed that the  $m \times m$  matrix  $\mathbf{A}$  is non-negative and primitive; hence there is a real and positive dominant eigenvalue  $\lambda$  that corresponds to the population growth rate. For detailed definition and examples of matrix models (see Caswell, 2001).

As an example, consider the matrix model for scentless chamomile (SC) from de Camino-Beck and Lewis (2007). Fig. 1 describes the scentless chamomile life cycle graph. The projection interval for this model is 1 year. Nodes 1, 2 and 3 correspond to seeds, rosettes and flowering plant stages. In the life cycle, seeds can germinate and produce either rosettes (stage without flowers) or flowering plants, or stay in the seed bank. Rosettes can survive over winter producing a flowering plant next year. The projection matrix of scentless chamomile is given by

$$\mathbf{A} = \begin{bmatrix} a_{11} & 0 & a_{13} \\ a_{21} & 0 & a_{23} \\ a_{31} & a_{32} & a_{33} \end{bmatrix} \quad (6)$$

Since only seeds disperse (the third column of the matrix), the dispersal matrix is given by difference kernels

$$\tilde{\mathbf{K}}(x_i, x_j) = \tilde{\mathbf{K}}(x_i - x_j) = \begin{bmatrix} \Delta(x_i - x_j) & \Delta(x_i - x_j) & \tilde{k}(x_i - x_j) \\ \Delta(x_i - x_j) & \Delta(x_i - x_j) & \tilde{k}(x_i - x_j) \\ \Delta(x_i - x_j) & \Delta(x_i - x_j) & \tilde{k}(x_i - x_j) \end{bmatrix}, \quad (7)$$

Here  $\tilde{k}(z)$ ,  $z = x - y$  is the dispersal kernel describing the dispersal of seeds and the discrete delta function  $\Delta(x_i - x_j)$ , defined as

$$\Delta(x_i - x_j) = \delta_{ij} = \begin{cases} 1, & \text{if } i = j \\ 0, & \text{otherwise} \end{cases}, \quad (8)$$

is used for transitions where no dispersal occurs. As can be seen from the third column of matrix  $\tilde{\mathbf{K}}(z)$ , seeds, produced by flowering plants, disperse and can remain as seeds, germinate to rosettes, or germinate to flowers in a single year.

A dispersal kernel can be defined using mechanistic principles, or can be obtained directly from data without assuming any particular shape (Lewis et al., 2005). Consider the example when relative frequencies of disperser  $f_j$ , are collected in two directions and at

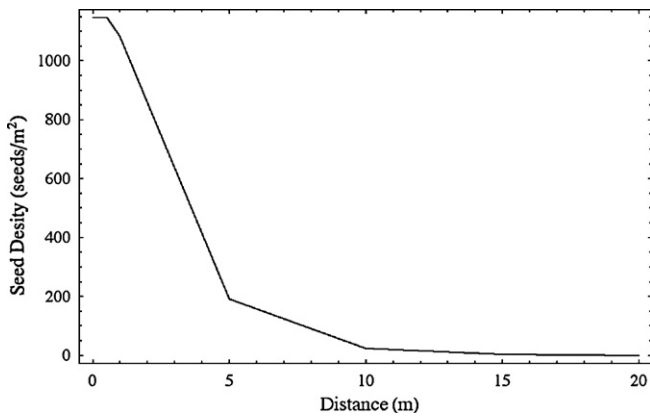


Fig. 2. Linear interpolation of the scentless chamomile data obtained as described in Appendix A.1. The data is obtained from the sum in all four cardinal directions, from seed traps collected in Vegreville, Alberta.

regular distances from a point source. With data points

$$\{(y_{-m}, f_{-m}), \dots, (y_{-2}, f_{-2}), (y_{-1}, f_{-1}), (y_1, f_1), (y_2, f_2), \dots, (y_m, f_m)\}, \tag{9}$$

where  $y_j$  is the location of the sample and  $f_j$  is the corresponding frequency, using a linear interpolation function, a continuous difference kernel suitable for an integro-difference model can be defined in terms of  $z = x - y$ ,

$$k(x, y) = k(z) = f_i + (f_i - f_{i-1}) \frac{z - y_i}{y_i - y_{i-1}} \quad \text{with } y_{i-1} < z < y_i. \tag{10}$$

As an example see Fig. 2, where the kernel shows absolute number of seeds.

A discrete kernel  $\tilde{k}(x, y)$  can come from discretizing a continuous kernel  $k(x, y)$  at any scale for use in terms of  $x_d = x_i - x_j$ ,

$$\tilde{k}(x_d) = \int_{x_d - (h/2)}^{x_d + (h/2)} k(z) dz, \quad -\infty < x_d < \infty. \tag{11}$$

In two dimensions, a radially symmetric matrix of kernels  $\mathbf{K}(\mathbf{x}, \mathbf{y}) = \mathbf{K}(r)$ ,  $r = \sqrt{z_1^2 + z_2^2}$ ,  $z_1 = x_1 - y_1$ ,  $z_2 = x_2 - y_2$  is discretized for use in a CML. With dispersal from  $(x_{j_1}, x_{j_2})$  to  $(x_{i_1}, x_{i_2})$  Eq. (11) can be written in terms of  $x_{d_1} = x_{i_1} - x_{j_1}$  and  $x_{d_2} = x_{i_2} - x_{j_2}$  as

$$\tilde{\mathbf{K}}(\mathbf{x}_d) = \int_{x_{d_1} - (h/2)}^{x_{d_1} + (h/2)} \int_{x_{d_2} - (h/2)}^{x_{d_2} + (h/2)} \mathbf{K} \left( \sqrt{z_1^2 + z_2^2} \right) dz_1 dz_2. \tag{12}$$

### 3. Population spread rates

The way invasive species move across space, and how fast this occurs, is essential in the understanding invasion processes and how they can be controlled. With matrix IDEs, it is possible to calculate the rate of spread of a local population. As described below, the rate of spread, denoted  $c^*$ , is calculated as the minimum possible wave speed  $c$  of a moving wave front. In this section, we first describe how these two quantities can be calculated for matrix IDEs, and then show how these calculations hold for matrix CMLs.

#### 3.1. Calculating rate of spread in a matrix CML

A quantity that can be computed when space is included is the rate of spatial spread of a population that has been introduced locally. The spread rate  $c^*$  is defined for a locally introduced population as follows. An observer moving along a ray oriented away from the local introduction will asymptotically observe a population density of zero if the movement speed is faster than  $c^*$  and

will asymptotically observe a positive population density if the speed is slower than  $c^*$ . A rigorous discussion and analysis of spread rates for structured population models can be found in Lui (1989). Neubert and Caswell (2000) showed for matrix integro-difference equations (matrix IDE), that the spread rate  $c^*$  can be related to the wave speed  $c(s)$  for an exponentially declining population density  $\mathbf{n}_t = \mathbf{w}e^{-s(x-ct)}$ .

CMLs can be considered a special case of matrix IDE, where space is discrete, therefore the dispersal kernel takes the shape of a function on a discrete lattice. To define wave speed, first we define the wave front and relate the discrete space CML with an associated exponential profile in a continuous space system (Fig. 3). We then show the derivation of the wave speed formula for discrete systems.

Similar to a matrix IDE, a wave speed formula can be derived for structured CML models. The derivation follows that of Neubert and Caswell (2000), but in this case we are dealing with discrete points on a lattice. Here, when deriving the wave speed, we are looking at a linear transition matrix in Eq. (4). In linear matrix CMLs the spread rate  $c^*$  of a locally introduced population can be calculated using the approach of Neubert and Caswell (2000) by evaluating the minimum possible wave speed  $c$  for an exponentially declining population density,

$$\mathbf{n}_t(x_i) = \mathbf{w}e^{-s(x_i-ct)}. \tag{13}$$

Substitution into (4) yields a formula that relates the speed of the wave  $c$  to the steepness of the wave  $s$  (as shown in Appendix A.2),

$$c(s) = \frac{1}{s} \ln(\rho_1(s)). \tag{14}$$

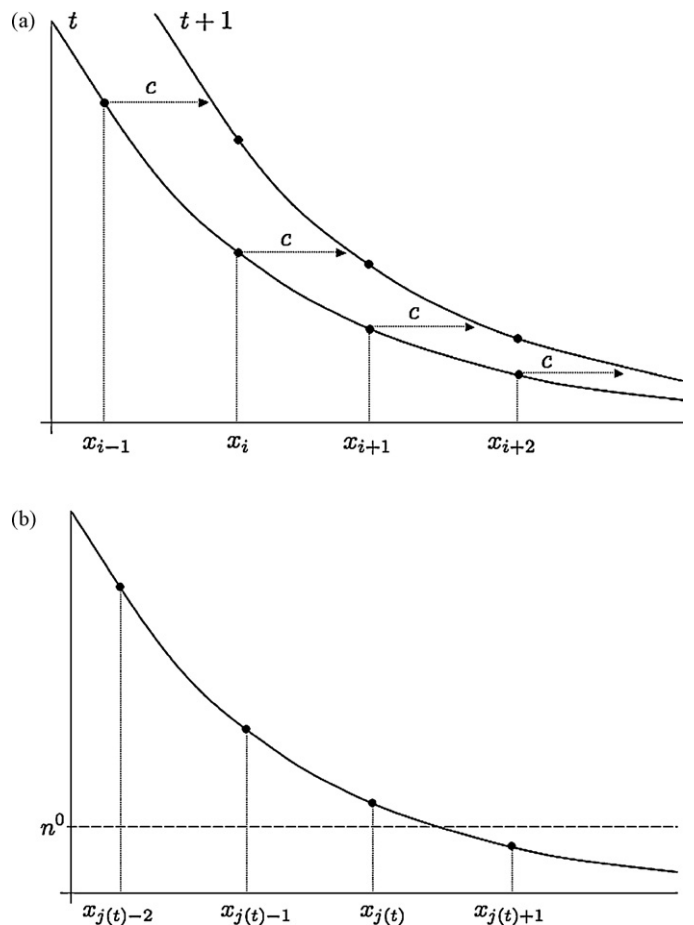


Fig. 3. (a) Associated exponential profile that moves a distance  $c \approx 0.9$  in one time step.  $n^0$  is the detection threshold. (b) The detection threshold  $n^0$  in the exponential profile is located between points  $x_{j(t)}$  and  $x_{j(t)+1}$ .

The spread rate for the locally introduced population is given as:

$$c^* = \min_{s>0} c(s), \tag{15}$$

where  $\rho_1(s)$  is the largest eigenvalue of  $\tilde{\mathbf{H}}(s) = \mathbf{A} \circ \tilde{\mathbf{M}}(s)$  and  $\tilde{\mathbf{M}}(s)$  is the matrix of generating functions:

$$\tilde{\mathbf{M}}(s) = \sum_{-\infty}^{\infty} \tilde{\mathbf{K}}(x_j) e^{sx_j}. \tag{16}$$

The formula for the spread rate Eq. (15) is proved rigorously in Lui (1989) in a general measure-theoretic context that includes both the discrete space setting (as given here) and the continuous space setting (as given in Neubert and Caswell, 2000). Fig. 3a shows the exponential profile and wave speed.

The spread on the lattice  $C_t$ , as calculated by the average rate of spatial extent of the spread over time, that is,  $C_t = x_{j(t)}/t$ , where  $x_{j(t)}$ , called spatial extent of spread, is the furthest point in the lattice where  $n(x_{j(t)}) \geq n^0$ ,  $n(x_{j(t)+1}) < n^0$  and  $n^0$  is the critical level where a site is considered not empty (Fig. 3b). Appendix A.2 shows that when the initial profile of the wave is exponentially decreasing with steepness  $s$ , it is possible to show that  $C_t \rightarrow c(s)$  as  $t \rightarrow \infty$ , where  $c(s)$  is the velocity of spread given in (14).

In summary, calculation of spread rate initially requires the transition matrix  $\mathbf{A}$  and kernel matrix  $\tilde{\mathbf{K}}$ . The kernel matrix is transformed to give a matrix of moment generating functions  $\tilde{\mathbf{M}}(s)$  by  $\mathbf{A}$ . This yields  $\tilde{\mathbf{H}}(s) = \mathbf{A} \circ \tilde{\mathbf{M}}(s)$ , whose dominant eigenvalue  $\rho_1(s)$ , is used in Eqs. (14) and (15) to calculate the spread rate  $c^*$ . Neubert and Caswell (2000) give a detailed derivation linking  $c^*$  to the minimum of  $c(s)$ .

For density-dependent projection matrices, the so-called *linear conjecture* states that the rate of spread of the matrix IDE model with density-dependent projection matrix  $\mathbf{A}_n$ , is governed by its linearization around  $\mathbf{n} = 0$  (Neubert and Caswell, 2000). In other words, even if there are nonlinear interactions in the population, the rate of spread is given by the growth and dispersal behaviour of the leading edge of the invasion, where  $\mathbf{n}$  is close to zero. Generally, this conjecture requires that there are no Allee effects at low population density. Some mathematical conditions under which the linear conjecture is known to hold are given in Lui (1989).

### 3.2. Calculating two-dimensional spread

A two-dimensional CML is defined as follows:

$$\mathbf{n}_{t+1}(\mathbf{x}_i) = \sum_{\mathbf{x}_j \in \Omega} [\tilde{\mathbf{K}}(\mathbf{x}_i - \mathbf{x}_j) \circ \mathbf{A}] \mathbf{n}_t(\mathbf{x}_j), \tag{17}$$

where  $\mathbf{n}_{t+1}(\mathbf{x}_i)$  now describes population density  $\mathbf{n}_{t+1}$  in location  $\mathbf{x}_j = [x_j \ y_j]^T$  in two dimensions, and  $\tilde{\mathbf{K}}(\mathbf{x}_i - \mathbf{x}_j)$ , as described earlier, is a matrix of kernels. Spread in two dimensions is calculated by considering only one direction, perpendicular to the wave front (see Lewis et al., 2005).

It turns out that it is the marginal distribution of this two dimensional kernel that is needed for calculating population spread (see also Lewis et al., 2005). In this case the marginal distribution can be calculated by summing over one direction to give

$$\tilde{\mathbf{K}}(x_{d_1}) = \sum_{x_{d_2}=-\infty}^{\infty} \tilde{\mathbf{K}}(\mathbf{x}_d), \tag{18}$$

with  $\mathbf{x}_d = [x_{d_1} \ x_{d_2}]^T$  (Fig. 4). The illustration in Fig. 5 shows the reason why probabilities are summed in one direction when the kernel is used in one dimension to describe two-dimensional spread. Fig. 4 shows the marginal distribution of a two-dimensional kernel.

Here we consider the case where spread is equal in all directions. Hence, Eq. (12) and Fig. 4 pertain.

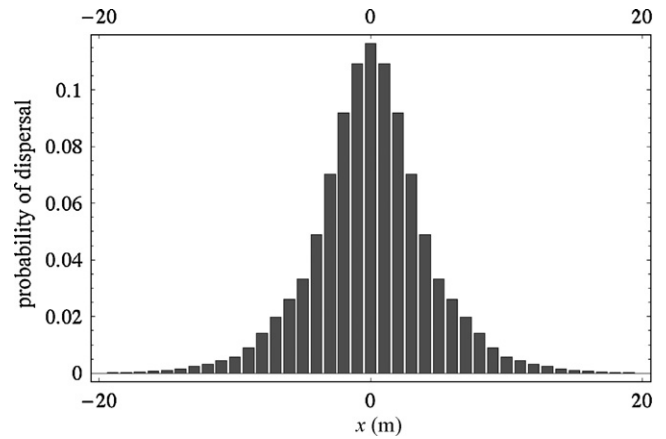


Fig. 4. Marginalized kernel for scentless chamomile data. The marginal distribution is taken on a two-dimensional kernel.

In summary, the marginal distribution of the kernel (Eq. (18) and Fig. 4) is used in calculating the matrix of generating functions (18). From this the spread rate  $c^*$  is calculated from (14) and (15).

### 3.3. Scentless chamomile rate of spread

Using the projection matrix in Eq. (6), and the kernel as defined in Eq. (10), it is possible to calculate the rate of spread for scentless chamomile. From field data collected in Vegreville, Canada in 2003–2005 (see Appendix A.1), the estimated projection matrix for scentless chamomile is given by:

$$\mathbf{A}_1 = \begin{bmatrix} 0.08 & 0 & 36376.45 \\ 0.27 & 0 & 517 \\ 0.04 & 0.45 & 297.85 \end{bmatrix},$$

$$\mathbf{A}_2 = \begin{bmatrix} 0.08 & 0 & 1775.22 \\ 0.27 & 0 & 25.24 \\ 0.04 & 0.45 & 14.53 \end{bmatrix}. \tag{19}$$

Because of this large difference between years, rate of spread will be calculated for both.

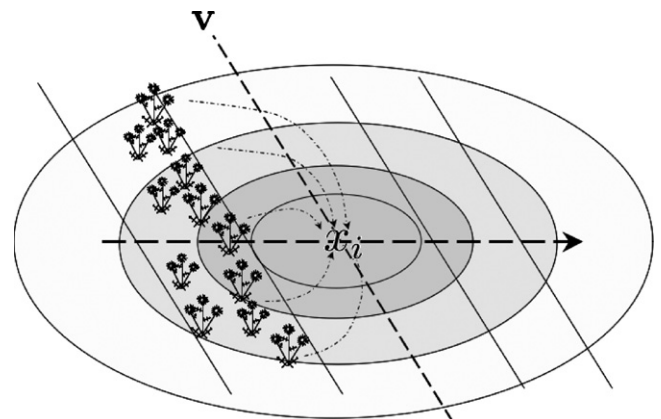
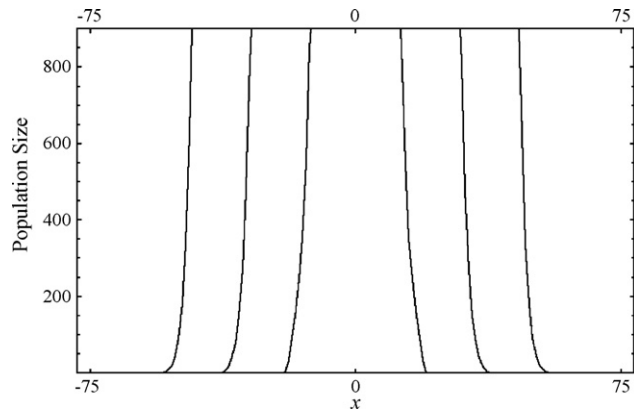


Fig. 5. This figure shows why the marginal distribution of the kernel is taken when analyzing spread in one dimension. Suppose position  $x_i$  is being updated, then propagules will arrive to location  $x_i$  in a two-dimensional system from all directions, with probability indicated by the concentric circles (the circles represent a kernel describing probabilities associated with points of origin  $\mathbf{x}_j$  for a seed dispersing to  $\mathbf{x}_i$ ,  $k(\mathbf{x}_j, \mathbf{x}_i)$ ). If spread is taken only in the direction of the dashed line, contributions from locations below and above have to be considered. Hence, when the system is analyzed in one direction  $\mathbf{u}$ , the contributions in direction  $\mathbf{v}$ , have to be summed. A precise mathematical derivation is given in Lewis et al. (2005).

**Table 1**  
Estimated rate of speed for scentless chamomile. The calculations were done with data described in Appendix A.1.

Method	c year 1	c year 2
Eq. (15)	$c^* = 16.55$ m/year	$c^* = 11.32$ m/year
Simulation in 1D	$c^* \approx 16.55$ m/year	$c^* \approx 11.32$ m/year
Bootstrap 90% CI	{16.43, 16.67}	{10.33, 12.10}



**Fig. 6.** Numerical simulation showing the front wave moving over time, in a one-dimensional simulation of the spread of scentless chamomile.

Using Eq. (15) we calculated the rate of spread for scentless chamomile to be  $c^* = 16.55$  m/year for year 1 and  $c^* = 11.32$  m/year for year 2. The numerical simulations of the spread rate and the 90% confidence intervals are shown in Table 1. The confidence intervals were obtained from bootstrapping the dispersal with a sample of 86 seeds. Fig. 6 shows the moving front in the one dimension numerical simulation.

#### 4. Incorporating heterogeneous landscape

Coupled map lattice models provide a convenient and direct way of linking real landscape information with the population model. The basic equation for growth and spread (Eq. (4)) with a difference kernel can be written in two spatial dimensions and modified to include growth or establishment constraints

$$\mathbf{n}_{t+1}(\mathbf{x}_i) = \mathbf{P}(\mathbf{x}_i) \circ \sum_{\mathbf{x}_j \in \Omega} [\mathbf{K}(\mathbf{x}_j - \mathbf{x}_i) \circ \mathbf{A}] \mathbf{n}_t(\mathbf{x}_j). \tag{20}$$

Here  $\mathbf{P}(\mathbf{x}_i)$  is a vector whose entries contain the probability of establishment of propagules in each stage in location  $\mathbf{x}_i = [x_i, y_i]^T$ . A landscape  $\mathbf{P}$  can be defined directly from a raster layer in a GIS system, as we will show later with an example.

It is expected that any spatial constraints will change the wave speed depending on the ability of the dispersers to travel long or short distances, and thus disperse in a fragmented landscape (With, 2004). Consider, for example, an invading organism that spreads quickly, diluting local populations. It may reduce global populations in a landscape where patches are too small, failing to establish stable populations in local patches. Hence, spatial inhomogeneities could be of consequence when designing control strategies.

To investigate spread of scentless chamomile (SC) through the landscape, we ran simulations of scentless chamomile on a real landscape. To run simulations on a landscape, we simplified the scentless chamomile system to an unstructured population model of the form:

$$n_{t+1}(\mathbf{x}_i) = P(\mathbf{x}_i) \sum_{\Omega} k(\mathbf{x}_i - \mathbf{x}_j) \lambda_1 n_t(\mathbf{x}_j), \tag{21}$$

where  $\lambda_1$  is the SC population growth rate for year 1, and  $P(\mathbf{x}_i)$  is the growth constraint in location  $\mathbf{x}_i$ . We use an unstructured model to simplify calculations and discussions, however, if detailed information exists on the effect of landscape on life stages, Eq. (20) can be used directly.

On the real landscape the discrete dispersal kernel was scaled using coarser 25 m bin sizes in Eq. (11) ( $3 \times 3$  cells in the landscape). The distances in the lattice are calculated from the center of the lattice point to the center of the adjacent lattice point. To illustrate the applicability of a CML model at a landscape level, we simulated spread using the estimated kernel over a 25 m resolution classified satellite image of the Vegreville-Edmonton region (Fig. 7), involving the area where the parameter estimates of the matrix mode were obtained, and dispersal data was collected. The classified image (Fig. 8a), shows pasture, cropland, forest, water bodies and infrastructure on a 25 m pixel resolution. Chamomile can grow in croplands, pastures, and infrastructure (road edges) (Bowes et al., 1994). The probability of establishment  $p$  were obtained from habitat occupancy reported for scentless chamomile in Saskatchewan ((Bowes et al., 1994), Table 2, samples from Balgonie, 1985). Based on occupancy probability,  $p$  for pastures was set to 0.6, cropland 0.024 and infrastructure 0.3. Results of the simulation are shown in Fig. 8. The simulations show the spread after 50, 150 and 300 iterations starting with an initial density of 1000 on a 25 m<sup>2</sup> area. Assuming spread equal in all directions, the velocity of spread was calculated using  $(1/t)(\sqrt{\text{area}/\pi})$ . The rate of spread for the heterogeneous landscape is 15.25 m/year compared to 22.25 m/year in the numerical simulation without constraints. The difference between the calculated  $c^* = 16.55$  m/year, and the numerical simulation without constraints, 22.25 m/year, is due to the scale at which the kernel was discretized. Coarser scales (larger  $h$ ) result in fatter kernels and therefore higher  $c^*$ .

#### 5. Environmental stochasticity

The matrix IDE and matrix CML model described assume temporal invariance in population growth and spread. However, in many cases this assumption is unrealistic (Neubert and Parker, 2004). Strong resource dependencies change local population dynamics and as a consequence, the ability of organisms to spread (Dwyer and Morris, 2006; Fagan et al., 2005). Chamomile results show how growth rate differs substantially from one year to the next one, and this difference also influences the rate of spread (Table 1).

The effect of these fluctuating environments can be incorporated by making population growth rate and the dispersal kernel a function of time (Neubert et al., 2000). For a CML,

$$\mathcal{N}_{t+1}(x_i) = \sum_{j=-\infty}^{\infty} [\tilde{\mathbf{K}}_t(x_i - x_j) \circ \mathbf{A}_t] \mathcal{N}_t(x_j). \tag{22}$$

Here  $\tilde{\mathbf{K}}_t(x_d)$ ,  $x_d = x_i - x_j$  is a matrix whose elements are independent, and identically distributed (i.i.d.) discrete dispersal kernels,  $\mathbf{A}_t$  are i.i.d. projection matrices, independent of the dispersal kernels for  $t = 0, 1, 2, \dots$ , and  $\mathcal{N}_t(x_i)$  is a stochastic process describing the density of individuals at grid point  $x_i$  and time  $t$ . In other words, for a given time  $t$  and lattice point  $x_i$ ,  $\mathcal{N}_{t+1}(x_i)$  is a vector of random variables describing the density of individuals from each stage.

Neubert et al. (2000) derived a formula to calculate the expected rate of spread and its variance for a stochastic scalar IDE. Here we derive formulae that can be used for stochastic matrix CMLs. As defined earlier,  $\tilde{\mathbf{H}}_t(s) = \tilde{\mathbf{M}}_t(s) \circ \tilde{\mathbf{A}}_t$  for  $t = 1, 2, \dots$ , where  $\tilde{\mathbf{H}}_t(s)$  is the matrix of generating functions for  $\tilde{\mathbf{K}}_t$  (see Eq. (16)). As in the earlier section  $\tilde{\mathbf{H}}_t(s)$  is a time-dependent non-negative and primitive matrix, with dominant eigenvalue  $\rho_{1t}(s)$  and corresponding eigenvector  $\mathbf{w}_{1t}(s)$ . Appendix A.3 shows that the random variable

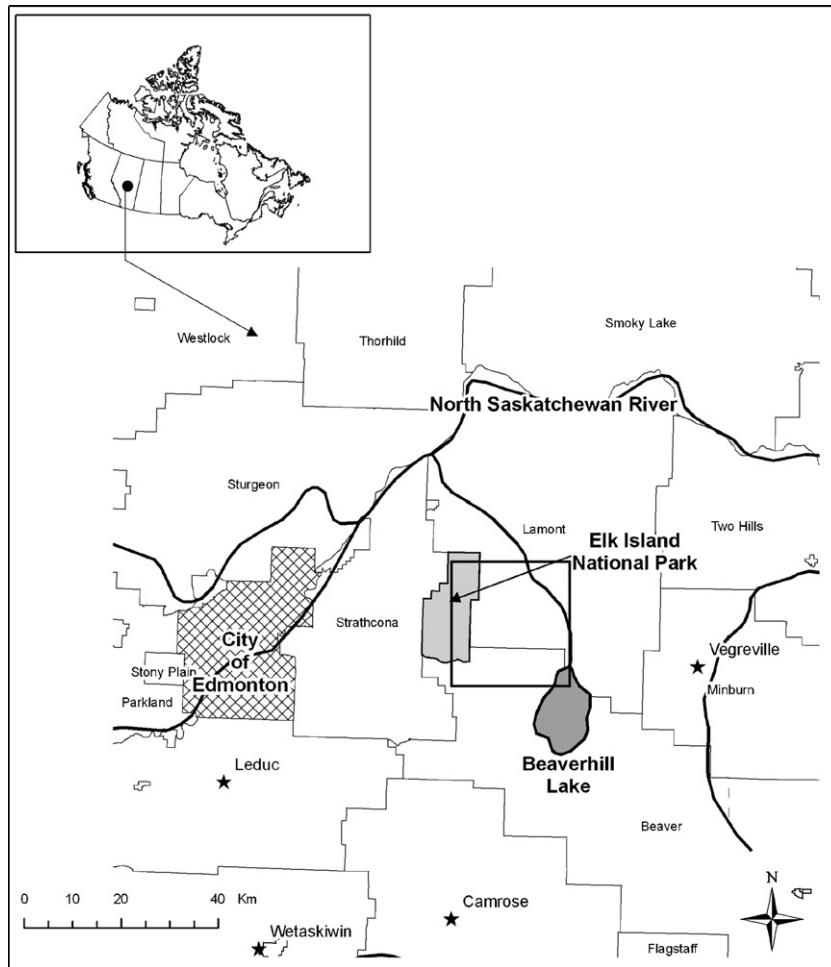


**Fig. 7.** Map of the Vegreville-Edmonton region. The thick line area indicates the subsection shown in Fig. 8. Map taken from Young et al. (2006) and edited with authors permission.

describing the spread rate  $C_t$  is given by  $C_t = \frac{x_j(t)}{t}$ . As  $t \rightarrow \infty$ ,

$$C_t = \frac{x_j(t)}{t} \rightarrow \frac{1}{s} \left( \frac{1}{t} \sum_{\tau=0}^{t-1} \ln(\rho_{1\tau}(s)) \right), \tag{23}$$

$C_t(s)$ , the mean of (40) up to time  $t$ , is evaluated using the dominant eigenvalue  $\rho_{1\tau}$  of the time-dependent matrix  $\tilde{\mathbf{H}}_{\tau}(s)$ . Because each eigenvalue is an i.i.d. random variable, and (23) calculates the mean of these from time  $\tau = 0$  to  $\tau = t - 1$ , the central limit theorem applies as  $t \rightarrow \infty$ . By the central limit theorem,  $C_t$  is normally distributed with mean

$$\mu(s) = E[\ln(\rho_{10})s^{-1}], \tag{24}$$

and variance

$$\sigma^2(s, t) = \frac{1}{t} \text{Var}[\ln(\rho_{10})s^{-1}], \tag{25}$$

for large time  $t$ .

As shown in Neubert et al. (2000) for scalar integro-difference equations, the expected spread rate for stochastic matrix CMLs is calculated as,

$$\bar{c}^* = \min_{s>0} \mu(s) = \mu(s^*). \tag{26}$$

Consider the scentless chamomile example. Fecundities were substantially different between year 1 and year 2, therefore there is one projection matrix for each year,  $\mathbf{A}_1$  and  $\mathbf{A}_2$  (19). As these were observed after two years we assume in the absence of any

other information that they are equally likely to occur. The kernels are kept constant. For large times  $t$  the average speed and variance are given by  $\mu(s^*)$  and  $\sigma^2(s^*, t)$  where the mean is

$$\mu(s) = \frac{1}{2s} [\ln(\rho_1(\tilde{\mathbf{H}}_1(s))) + \ln(\rho_1(\tilde{\mathbf{H}}_2(s)))], \tag{27}$$

and the variance is,

$$\sigma^2(s, t) = \frac{1}{t} \left[ \frac{1}{2s^2} \ln^2(\rho_1(\tilde{\mathbf{H}}_1(s))) + \ln^2(\rho_1(\tilde{\mathbf{H}}_2(s))) \right] - \mu^2(s), \tag{28}$$

and  $s^*$  is the wave steepness that minimizes (27) (see Eq. (26)). With

$$\tilde{\mathbf{H}}_1 = \mathbf{A}_1 \circ \begin{bmatrix} 1 & 1 & \tilde{\mathbf{M}}(s^*) \\ 1 & 1 & \tilde{\mathbf{M}}(s^*) \\ 1 & 1 & \tilde{\mathbf{M}}(s^*) \end{bmatrix}, \quad \tilde{\mathbf{H}}_2 = \mathbf{A}_2 \circ \begin{bmatrix} 1 & 1 & \tilde{\mathbf{M}}(s^*) \\ 1 & 1 & \tilde{\mathbf{M}}(s^*) \\ 1 & 1 & \tilde{\mathbf{M}}(s^*) \end{bmatrix}, \tag{29}$$

the expected spread rate calculated using Eq. (26), is  $\bar{c}^* = 14.29$  and its variance  $\sigma^2(s^*, t) = 196.9/t$ . Fig. 9 shows the calculated wave speed  $C_t$  and wave speed variance  $\sigma^2(t)$ , for 20 realizations of the numerical simulations. As seen in the figure,  $C_t$  converges to the calculated  $\bar{c}^*$  and the variance decreases according to (28) as time increases.

### 6. Discussion

We showed that the wave speed and rate of spread can be calculated for matrix CMLs in constant and stochastic environments in one and two dimensions. We also showed how heterogeneous landscape information can be incorporated to the CML model. Using

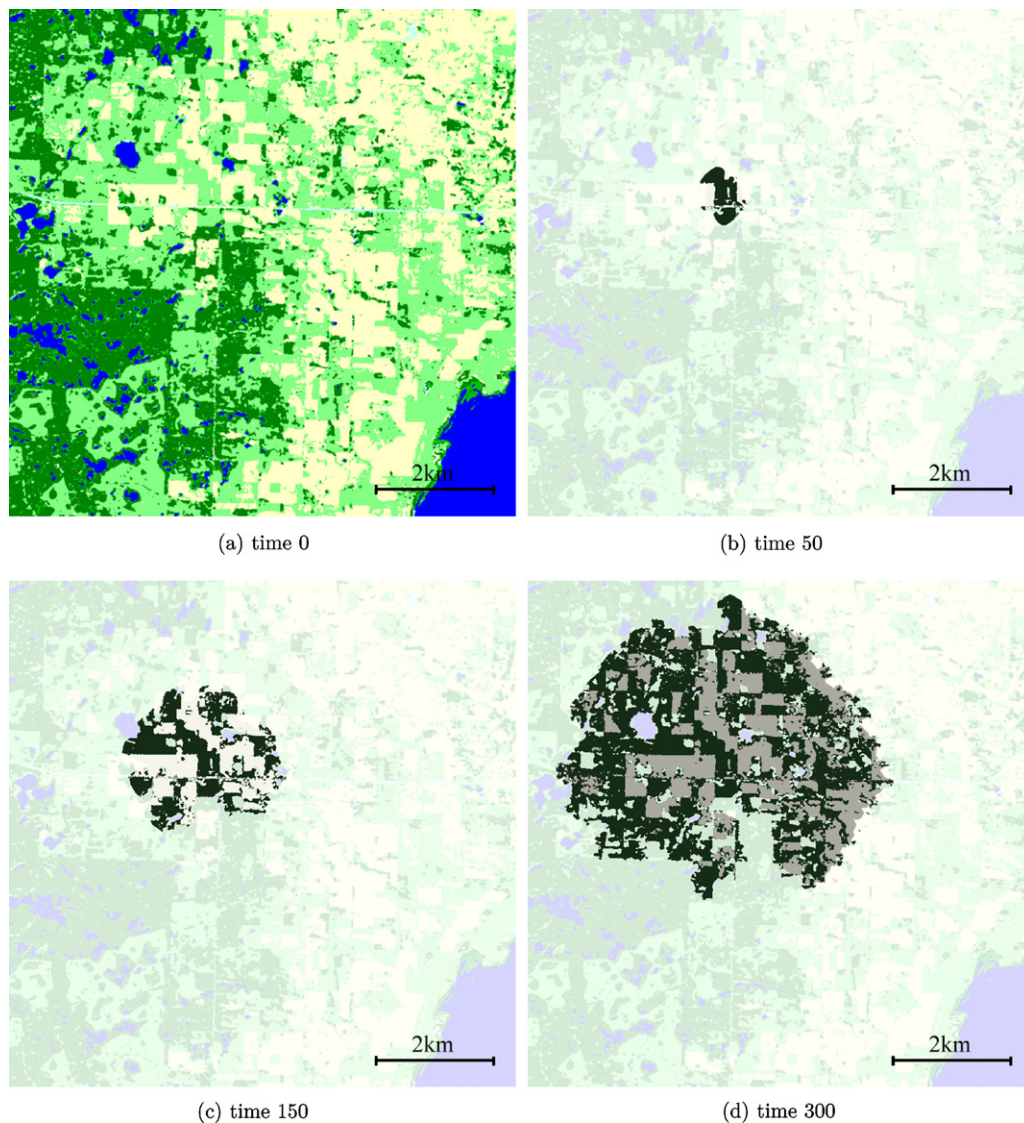


**Fig. 8.** Numerical simulations of Eq. (20) on a real landscape, the land uses classes correspond to, blue: water, dark green: forest, light green: pastures, yellow: cropland, light blue: infrastructure. (a) Landscape corresponds to a subsection of Fig. 7, (b) simulation after 50 years, (c) simulation of Eq. (20) parameterized for scentless chamomile after 150 iterations, and (d) 300 iterations. Shades of grey show scentless chamomile density. (For interpretation of the references to colour in this figure legend, the reader is referred to the web version of the article.)

scentless chamomile as an example, we showed how these methods can be applied.

### 6.1. Matrix coupled map lattices

Coupled map lattices are a convenient way of modelling spatial dynamics of invasive species. In these models population structure, age or stage structured, and spatial dynamics, using discrete kernels; can be incorporated to calculate vital quantities in biological invasion. The main result of this paper is a CML framework for calculating rates of spread in constant, heterogeneous and stochastic environments. The methods shown here, calculation of rate of spread in stochastic and constant environments, are tools already developed for scalar and matrix IDEs (Kot et al., 1996; Neubert et al., 2000; Neubert and Caswell, 2000).

There are few examples of CMLs being used for biological invasions. In most cases, the CML have been used informally to incorporate heterogeneous landscape information and study distribution patterns, and not to calculate spread. Bjornstad and Bascompte (2001), for example, build a CML to understand how

the self-organizing spatial patterns emerge; and Rees and Paynter (1997), build a spatially explicit structured models that studies the ground covered by scotch broom. These models do not formulate the calculation of rate of spread, nor do they allow for analytical work due to their complexity. Individual-based models have been a choice for modelling spread in heterogeneous environment, but their results are not amenable to general analysis, like formal differential equations or integro-difference equation models (Hastings et al., 2005).

The formulae derived here are summarized in Table 2. The quantity  $c^*$  is the biologically relevant statistic. If an individual viewing the invasion moves faster than  $c^*$ , it will outrun the invasion. On the other hand if it moves slower than  $c^*$  then it will fall behind. The calculation of  $c^*$  is done using the related wave speed quantity  $c(s)$ . This quantity describes the speed of a declining profile  $n_t(x) \propto \exp(-s(x - ct))$ , where the speed is a function of the steepness of the wave  $s$ . The relation between  $c^*$  and  $c(s)$  was initially investigated by Aronson and Weinberger (1978) for Fisher's equation. They showed that the rate of spread is obtained by minimizing  $c(s)$  over all possible values of steepness  $s$ . The same holds for both

**Table 2**  
Rate of spread formulae.

Symbol	Description	Formula	Source
$c(s)$	Wave speed for matrix IDEs, and matrix CMLs	(14)	Neubert and Caswell (2000) (IDE) and this paper (CML)
$c^*$	Spread rate for matrix IDEs and matrix CMLs	(15)	Neubert and Caswell (2000) (IDE) and this paper (CML)
$C_t$	Average rate of spatial extent of spread fro matrix IDEs and matrix CMLs	(40)	Neubert and Caswell (2000) (IDE) and this paper (CML)
$\bar{C}_t$	Average rate of spatial extent of spread stochastic matrix CMLs	(23)	This paper
$\hat{c}^*$	Expected spread rate for stochastic matrix CMLs	(26)	This paper

matrix IDEs (Neubert and Caswell, 2000), and for matrix CMLs (see Lui, 1989, for the general proof).

The assumption that environments are constant over time is unrealistic. For that,  $C_t$ , a random variable describing the average rate of spatial extent can be used. It is possible to calculate the mean and variance for  $C_t$ , for large time.

6.2. Lessons for the design of control strategies

Matrix CMLs can be a useful tool for the design of control strategies, because they allow one to:

- (1) Calculate demographic parameters,  $\lambda$ ,  $R_0$ , and rate of spread  $c^*$ .
- (2) Determine how fast a pest is spreading and what aspects of the life history of the invader should be target of control.
- (3) Establish how landscape heterogeneity, using real landscape information from GIS, affects the rate of spread of the invader.
- (4) Incorporate environmental stochasticity and study the effect of control strategies reducing spread.

- (5) Focus on measurable local dispersal data, rather than long-distance human-mediated dispersal.
- (6) Potentially use the CML model to optimize strategies in space and time to minimize  $c^*$  and  $\lambda$  with minimum effort.

Although matrix CMLs and other models of spatial dynamics, are a simplified representation of the invasion process, assuming the basic dynamic is well defined in these models, they can serve as useful tools to focus control of invasive species research.

Acknowledgements

We thank Marjorie Wonham, Alex Potapov, Alec McClay, and the Lewis Lab for discussions, comments, and revisions on the manuscript. We also thank the Jason Young at the University of Alberta Biosciences GIS Facilities for providing GIS data. T.de-C.-B. was supported by MITACS, University of Alberta Studentship, NSERC Discovery grand, and NSERC Collaborative research opportunity grant. M.A.L. gratefully acknowledges support from NSERC Discovery grant, NSERC Collaborative research opportunity grant and Canada Research Chair.

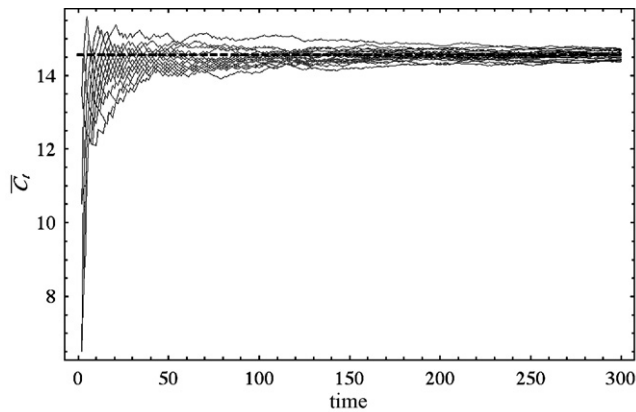
Appendix A.

A.1. Scentless chamomile field data

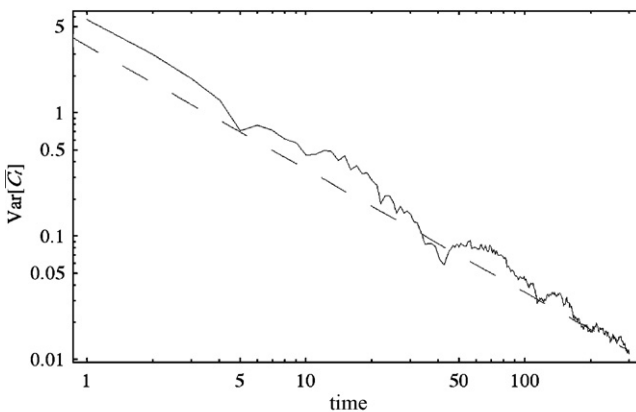
Parameter estimates of the transition matrix entries  $a_{ij}$  were obtained from field work and the literature estimates as follows. In the 32 plots established, a cohort in an inner 1 m × 1 m plot was followed for 3 years. The first year (2003), all emerging scentless chamomile plants were counted, these plants were assumed to have germinated from the seed bank and not from additional sources (dispersal). At the end of the year all rosettes and flowering plants were counted and all flowering plants were clipped, transition  $a_{31}$  was calculated from the number of flowering plants that year, and  $a_{21}$  from all scentless chamomile plants that had no flowers. The second year (2004), only surviving over-wintering rosettes remained. There were no new emerging plants. Transition  $a_{32}$  was estimated from the number of rosettes that produced flowers at the end of the year. The number of flowering heads were counted in the clipped treatments. The third year (2005) included rosettes and flowering plants, all flowering heads were removed and counted in September 2005. The total fecundity ( $a_{13} + a_{23} + a_{33}$ ) was obtained from the flower counts and image data for 2004 and from flower counts on 2005 (see Table 3). To differentiate between transitions  $a_{13}$ ,  $a_{23}$ ,  $a_{33}$  the number of seeds for each transition was estimated

**Table 3**  
Transition matrix parameter estimation. S: seed bank, R: rosettes, and F: flowering plants.

Transition	Description	Source
$a_{11}$	SB survival	Hinz (1999)
$a_{21}$	SB to R	Emerging R year 1
$a_{31}$	SB to F	Emerging F year 1
$a_{32}$	R to F	Surviving R to F year 2
$a_{13}, a_{23}, a_{33}$	F to SB,R,F	Field data. Proportional to Hinz (1999)



(a) Velocity of spread.



(b) Velocity of spread variance.

**Fig. 9.** Estimated velocity of spread and variance for 20 realization of the stochastic model. The simulations were run 20 iterations. The dashed line indicates  $\hat{c}$  obtained using Eq. (26).

using the same transition probabilities of seeds going to the seed bank, rosettes or flowering plants, found by Hinz (1999).

To estimate the dispersal ability of scentless chamomile, two healthy plants were transplanted from the Alberta Research Council (ARC) green house in Vegreville, to a hay field in July 2004. Each plant had 222 and 232 flowering heads with an average of 330 seeds/head. For each plant, 10 cm diameter, 10 cm deep, seed traps were placed in the North, East, South, West directions at distances of 0.5, 5, 10, 15 and 20 m from the source plant. Seeds were collected the following year in late spring and manually counted.

A.2. CML wave speed

When the initial profile of the wave is exponentially decreasing with steepness  $s$ , it is possible to show that  $C_t \rightarrow c(s)$  as  $t \rightarrow \infty$ , where  $c(s)$  is the velocity of spread given in (14). For an initial condition of the form:

$$\mathbf{n}_0(x_i) = \mathbf{n}^0 e^{-sx_i}, \tag{30}$$

any solution to (4) can be written in term of eigenvalues  $\rho_i(s)$  and eigenvectors  $\mathbf{w}_i(s)$  of  $\mathbf{H}(s)$  as

$$\mathbf{n}_t(x_i) = [\beta_1 \rho_1(s)^t \mathbf{w}_1(s) + \beta_2 \rho_2(s)^t \mathbf{w}_2(s) + \dots + \beta_n \rho_n(s)^t \mathbf{w}_n(s)] e^{-sx_i}. \tag{31}$$

Dividing by  $\rho_1(s)^t$  we get,

$$\frac{\mathbf{n}_t(x_i)}{\rho_1(s)^t} = \left[ \beta_1 \mathbf{w}_1(s) + \beta_2 \left( \frac{\rho_2(s)}{\rho_1(s)} \right)^t \mathbf{w}_2(s) + \dots + \beta_n \left( \frac{\rho_n(s)}{\rho_1(s)} \right)^t \mathbf{w}_n(s) \right] e^{-sx_i}. \tag{32}$$

Because  $\rho_1$  is the largest eigenvalue, as  $t \rightarrow \infty$ ,

$$\frac{\mathbf{n}_t(x_i)}{\rho_1(s)^t} = \beta_1 \mathbf{w}_1(s) e^{-sx_i}, \tag{33}$$

where  $\mathbf{w}_1(s)$  is the left eigenvector of  $\mathbf{H}(s)$  and gives the stable stage distribution in the spreading population and  $s$  is the steepness of the advancing edge of the wave. Rearranging Eq. (33),

$$\mathbf{n}_t(x_i) = \beta_1 \mathbf{w}_1(s) e^{-sx_i} \rho_1(s)^t. \tag{34}$$

Without loss of generality, we consider any component  $n_t$  of  $\mathbf{n}_t$  with corresponding eigenvector component  $w_1$ . Since we are dealing with a discrete lattice rather than the real line, at time  $t$ ,  $n^0$  lies somewhere between discrete points  $x_{j(t)}$  and  $x_{j(t)+1}$  (Fig. 3b). Hence,

$$\beta_1 w_1(s) e^{-sx_{j(t)}} \rho_1(s)^t \leq n^0 \leq \beta_1 w_1(s) e^{-sx_{j(t)+1}} \rho_1(s)^t, \tag{35}$$

which can be rewritten,

$$e^{-sx_{j(t)}} \leq \frac{n^0}{\beta_1 w_1(s)} \rho_1(s)^{-t} \leq e^{-sx_{j(t)+1}}. \tag{36}$$

Taking natural logarithms and dividing by  $s$  gives

$$-x_{j(t)} \leq \frac{1}{s} \ln \left( \frac{n^0}{\beta_1 w_1(s)} \right) - \frac{t}{s} \ln(\rho_1(s)) \leq -x_{j(t)+1}, \tag{37}$$

and dividing by  $-t$  yields

$$\frac{x_{j(t)}}{t} \geq \frac{1}{st} \ln \left( \frac{n^0}{\beta_1 w_1(s)} \right) + \frac{\ln(\rho_1(s))}{s} \geq \frac{x_{j(t)}}{t} - \frac{h}{t}, \tag{38}$$

which can be rewritten,

$$\frac{1}{st} \ln \left( \frac{n^0}{\beta_1 w_1(s)} \right) + \frac{\ln(\rho_1(s))}{s} \leq \frac{x_{j(t)}}{t} \leq \frac{1}{st} \ln \left( \frac{n^0}{\beta_1 w_1(s)} \right) + \frac{\ln(\rho_1(s))}{s} + \frac{h}{t}. \tag{39}$$

As  $t \rightarrow \infty$  the left and right quantities in the above equation approach  $\frac{1}{s} \ln(\rho_1(s))$ , the spread rate  $C_t$  is defined as,

$$C_t = \frac{x_{j(t)}}{t} \rightarrow \frac{1}{s} \ln(\rho_1(s)) = c(s), \tag{40}$$

as in Eq. (14).

A.3. Wave speed for stochastic environment matrix CMLs

In this Appendix we show that with an initial condition of the form  $\mathbf{n}_0 = \mathbf{n}^0 e^{-sx}$ , solutions to (22) can be written as a linear combination,

$$\mathcal{N}_1(x_i) = [\beta_{10} \rho_{10}(s) \mathbf{w}_{10}(s) + \beta_{20} \rho_{20}(s) \mathbf{w}_{20}(s) + \dots] e^{-sx_i} \tag{41}$$

$$\mathcal{N}_2(x_i) = [\beta_{11} \rho_{10}(s) \rho_{11}(s) \mathbf{w}_{11}(s) + \beta_{20} \rho_{20}(s) \rho_{21}(s) \mathbf{w}_{21}(s) + \dots] e^{-sx_i} \tag{42}$$

⋮

$$\mathcal{N}_t(x_i) = \left[ \beta_{1t-1} \left( \prod_{\tau=0}^{t-1} \rho_{1\tau}(s) \right) \mathbf{w}_{1t-1}(s) + \dots \right] e^{-sx_i}. \tag{43}$$

Dividing by  $\prod_{\tau=0}^{t-1} \rho_{1\tau}(s)$ , and since  $\rho_{1\tau}(s)$  are the largest eigenvalues, as  $t \rightarrow \infty$ ,

$$\mathcal{N}_t(x_i) \rightarrow \beta_{1t-1} \mathbf{w}_{1t-1}(s) e^{-sx_i} \left( \prod_{\tau=0}^{t-1} \rho_{1\tau}(s) \right)^{-1}. \tag{44}$$

Without loss of generality, consider any component  $\mathcal{N}_t$  of  $\mathcal{N}_t$  with corresponding eigenvector component  $\mathbf{w}_{1t-1}(s)$ . In the lattice at time  $t$ ,  $n^0$  lies somewhere between discrete points  $x_{j(t)}$  and  $x_{j(t)+1}$  (Fig. 3). Hence,

$$\mathcal{N}_t(x_{j(t)}) \leq n^0 \leq \mathcal{N}_t(x_{j(t)+1}), \tag{45}$$

which can be written,

$$e^{-sx_{j(t)}} \leq \frac{n^0}{\beta_{1t-1} w_{1t-1}(s)} \left( \prod_{\tau=0}^{t-1} \rho_{1\tau}(s) \right)^{-1} \leq e^{-sx_{j(t)+1}}. \tag{46}$$

Taking the natural logarithms and dividing by  $-st$  yields,

$$\frac{1}{st} \ln \left( \frac{n^0}{\beta_{1t-1} w_{1t-1}(s)} \right) + \frac{1}{s} \left( \frac{1}{t} \sum_{\tau=0}^{t-1} \ln(\rho_{1\tau}(s)) \right) \leq \frac{x_{j(t)}}{t} \tag{47}$$

$$\leq \frac{1}{st} \ln \left( \frac{n^0}{\beta_{1t-1} w_{1t-1}(s)} \right) + \frac{1}{s} \left( \frac{1}{t} \sum_{\tau=0}^{t-1} \ln(\rho_{1\tau}(s)) \right) + \frac{h}{t}. \tag{48}$$

The spread rate  $C_t = x_{j(t)}/t$  is now a random variable. As  $t \rightarrow \infty$ ,

$$C_t = \frac{x_{j(t)}}{t} \rightarrow \frac{1}{s} \left( \frac{1}{t} \sum_{\tau=0}^{t-1} \ln(\rho_{1\tau}(s)) \right), \tag{49}$$

$C_t(s)$ , the mean of (40) up to time  $t$ , evaluated using the dominant eigenvalue  $\rho_{1\tau}$  of the time-dependent matrix  $\tilde{\mathbf{H}}_t(s)$ .

References

Allen, L., Allen, E., Ponweera, S., 1996. A mathematical model for weed dispersal and control. *Bulletin of Mathematical Biology* 58 (Sep), 815–834.  
 Aronson, D., Weinberger, H., 1978. Multidimensional non-linear diffusion arising in population-genetics. *Advances In Mathematics* 30, 33–76.  
 Bjornstad, O., Bascompte, J., 2001. Synchrony and second-order spatial correlation in host-parasitoid systems. *Journal of Animal Ecology* 70 (Nov), 924–933.  
 Bonsall, M., Hassell, M., 2000. The effects of metapopulation structure on indirect interactions in host-parasitoid assemblages. *Proceedings of The Royal Society of London Series B—Biological Sciences* 267 (Nov), 2207–2212.  
 Bowes, G., Spurr, D., Thomas, A., Peschken, D., Douglas, D., 1994. Habitats occupied by scentless chamomile (*Matricaria perforata* Merat) in Saskatchewan. *Canadian Journal of Plant Science* 74 (2), 383–386.

- Brannstrom, A., Sumpter, D., 2005. Coupled map lattice approximations for spatially explicit individual-based models of ecology. *Bulletin of Mathematical Biology* 67 (Jul), 663–682.
- Buckley, Y., Brockerhoff, E., Langer, L., Ledgard, N., North, H., Rees, M., 2005. Slowing down a pine invasion despite uncertainty in demography and dispersal. *Journal of Applied Ecology* 42, 1020–1030.
- Caswell, H., 2001. *Matrix Population Models: Construction, Analysis, and Interpretation*, 2nd edition. Sinauer Associates.
- de-Camino-Beck, T., Lewis, M.A., 2007. A new method for calculating net reproductive rate from graph reduction with application to the control of invasive species. *Bulletin of Mathematical Biology* 69 (4), 1341–1354.
- Durrett, R., Levin, S., 1994. Stochastic spatial models—a users guide to ecological applications. *Philosophical Transactions of The Royal Society of London Series* 343 (Feb), 329–350.
- Dwyer, G., Morris, W., 2006. Resource-dependent dispersal and the speed of biological invasions. *American Naturalist* 167 (Feb), 165–176.
- Fagan, W., Lewis, M., Neubert, M., Aumann, C., Apple, J., Bishop, J., 2005. When can herbivores slow or reverse the spread of an invading plant? A test case from Mount St. Helens. *American Naturalist* 166 (Dec), 669–685.
- Fagan, W., Lewis, M., Neubert, M., Van Den Driessche, P., 2002. Invasion theory and biological control. *Ecology Letters* 5 (1), 148–157.
- Hassell, M., Comins, H., May, R., 1991. Spatial structure and chaos in insect population-dynamics. *Nature* 353 (6341), 255–258.
- Hastings, A., Cuddington, K., Davies, K., Dugaw, C., Elmendorf, S., Freestone, A., Harrison, S., Holland, M., Lambrinos, J., Malvadkar, U., Melbourne, B., Moore, K., Taylor, C., Thomson, D., 2005. The spatial spread of invasions: new developments in theory and evidence. *Ecology Letters* 8 (Jan), 91–101.
- Hinz, H., 1996. International Symposium on Biological Control of Weeds: Proceedings of the IX International Symposium on Biological Control of Weeds. Ch. Scentless chamomile, a target weed for biological control in Canada: factors influencing seedling establishment, pp. 187–192.
- Hinz, H., 1999. Prospects for the classical biological control of *Tripleurospermum perforatum* in north America. Ph.D. thesis, Freigurg-Schweiz University.
- Hinz, H., McClay, A., 2000. Ten years of scentless chamomile: prospects for the biological control of a weed of cultivated land. In: *Proceedings of the X International Symposium on Biological Control of Weeds*, pp. 537–550.
- Janosi, I., Scheuring, I., 1997. On the evolution of density dependent dispersal in a spatially structured population model. *Journal of Theoretical Biology* 187 (Aug), 397–408.
- Jiang, M., Zhang, Q., 2008. A coupled map lattice model of tree dispersion. *Discrete and Continuous Dynamical Systems—Series B* 9 (Jan (1)), 83–101.
- Kaneko, K., 1992. Overview of coupled map lattices. *Chaos* 2 (3), 279–282.
- Kean, J., Barlow, N., 2001. A spatial model for the successful biological control of *Sitona Discoides* by *Microctonus Aethiopoidea*. *Journal of Applied Ecology* 38 (1), 162–169.
- Kot, M., Lewis, M., van den driessche, P., 1996. Dispersal data and the spread of invading organisms. *Ecology* 77 (7), 2027–2042.
- Lewis, M., Neubert, M., Caswell, H., Clark, J., Shea, K., 2005. A guide to calculating discrete-time invasion rates from data. In: *Conceptual Ecology and Invasions Biology*. Springer.
- Lui, R., Apr 1989. Biological growth and spread modeled by systems of recursions. 1. Mathematical-theory. *Mathematical Biosciences* 93, 269–295.
- McLeod, S., Saunders, G., 2001. Improving management strategies for the red fox by using projection matrix analysis. *Wildlife Research* 28 (4), 333–340.
- Neubert, M., Caswell, H., 2000. Demography and dispersal: calculation and sensitivity analysis of invasion speed for structured populations. *Ecology* 81 (6), 1613–1628.
- Neubert, M., Kot, M., Lewis, M., 2000. Invasion speeds in fluctuating environments. *Proceedings of the Royal Society of London Series B—Biological Sciences* 267 (1453), 1603–1610.
- Neubert, M., Parker, I., 2004. Projecting rates of spread for invasive species. *Risk Analysis* 24 (Aug), 817–831.
- Parker, I., 2000. Invasion dynamics of *Cytisus scoparius*: a matrix model approach. *Ecological Applications* 10 (3), 726–743.
- Rees, M., Hill, R., 2001. Large-scale disturbances, biological control and the dynamics of gorse populations. *Journal of Applied Ecology* 38 (2), 364–377.
- Rees, M., Paynter, Q., 1997. Biological control of scotch broom: modelling the determinants of abundance and the potential impact of introduced insect herbivores. *Journal of Applied Ecology* 34 (Oct), 1203–1221.
- Shea, K., 2004. Models for improving the targeting and implementation of biological control of weeds. *Weed Technology* 18, 1578–1581.
- Shea, K., Kelly, D., 1998. Estimating biocontrol agent impact with matrix models: *Carduus nutans* in New Zealand. *Ecological Applications* 8 (3), 824–832.
- van den Driessche, P., Watmough, J., 2002. Reproduction numbers and sub-threshold endemic equilibria for compartmental models of disease transmission. *Mathematical Biosciences* 180 (Nov), 29–48.
- White, S., White, K., 2005. Relating coupled map lattices to integro-difference equations: dispersal-driven instabilities in coupled map lattices. *Journal of Theoretical Biology* 235 (Aug), 463–475.
- With, K., 2004. Assessing the risk of invasive spread in fragmented landscapes. *Risk Analysis* 24 (Aug), 803–815.
- Young, J.E., Sanchez-Azofeifa, G., Hannon, S., Chapman, R., 2006. Trends in land cover change and isolation of protected areas at the interface of the southern boreal mixedwood and aspen parkland in Alberta, Canada. *Forest Ecology and Management* 230 (1–3) 151–161.